DOI 10.1007/978-1-4939-2038-9_17
Reprinted from *Solar Physics* Journal, DOI 10.1007/s11207-014-0503-0

A Reconstruction of Ultraviolet Spectral Irradiance During the Maunder Minimum

C. Bolduc · P. Charbonneau · R. Barnabé · M.S. Bourqui

Received: 10 July 2013 / Accepted: 12 February 2014 / Published online: 5 March 2014

Abstract We present a reconstruction of the solar spectrum in the near and mid-ultraviolet spectral range during the Maunder Minimum, a period of strongly suppressed magnetic activity spanning the second half of the 17th century. This spectral reconstruction is based on an extension of the Monte Carlo Solar Spectral Irradiance Model (MOCASSIM). The new version of the model, documented in this paper, extends its spectral range down to 150 nm, its temporal range back to 1610, includes a secular modulation of the quiet-Sun emissivity based on a total solar irradiance reconstruction, and uses the *Atmospheric Laboratory for Applications and Science-3* (ATLAS-3) spectrum as a reconstruction baseline. The model is validated against the ATLAS-1 spectrum for 29 March 1992, showing a general agreement varying from ~ 1 % in the 300 – 400 nm range, up to 3 – 5 % below 200 nm, the largest discrepancies occurring in emission lines formed in the chromosphere and transition region. We also reconstruct ultraviolet spectra for May 2008 and March 2009, spanning the extended phase of low activity separating Cycles 23 and 24. Our results suggest that despite the unusually long temporal extent of this activity minimum, the ultraviolet emission still remained slightly higher than during the Maunder Minimum, due to the lingering presence of decay products from active regions having emerged in the late descending phase of Cycle 23.

Keywords Solar irradiance · Spectrum, ultraviolet

C. Bolduc (✉) · P. Charbonneau · R. Barnabé · M.S. Bourqui
Département de Physique, Université de Montréal, C.P. 6128, succursale Centre-Ville, Montréal, Québec, H3C 3J7, Canada
e-mail: cassandra@astro.umontreal.ca

P. Charbonneau
e-mail: paulchar@astro.umontreal.ca

R. Barnabé
e-mail: roxane.barnabe@umontreal.ca

M.S. Bourqui
e-mail: michel.bourqui@mcgill.ca

1. Introduction

Observations of solar spectral irradiance (SSI) in the ultraviolet have shown that its variability over the course of the magnetic activity cycle is much larger than the ~ 0.1 % characterizing total solar irradiance (TSI). For example, the spectra obtained by the *SOLar SPECtrum* (SOLSPEC) instrument on the *Atmospheric Laboratory for Applications and Science* (ATLAS) 1 and 3 missions by Thuillier *et al.* (2003) at epochs of high and low solar activity, respectively, reveal that the variability increases rapidly with decreasing wavelength, from about 1 % at 300 nm up to 10 % around 150 nm. In itself, the direct impact of TSI variability on climate is probably too low to account for global warming measured in recent decades. Even though the effects of SSI variability on the stratosphere, combined with surface effects by TSI variability, are now thought to impact significantly on the troposphere, with the stratosphere acting as an amplifier of solar variability (Haigh *et al.*, 2010), the change in solar irradiance cannot explain the recent increase in global temperature (Forster *et al.*, 2007). It is widely accepted that anthropogenic forcing is responsible for the recent global warming and that the contribution from the solar forcing is very low in comparison, especially considering that solar activity has been decreasing over the past decade. However, before the beginning of the industrial era, when anthropogenic forcing was negligible, the SSI variability might have had an important influence on climate. One striking example is the coincidence of the Maunder Minimum, during which solar activity (and possibly solar irradiance) was very reduced, and the Little Ice Age, during which temperatures were noticeably colder, especially in the northern hemisphere (Gray *et al.*, 2010).

The understanding of the physical mechanisms implied and their mutual interactions necessitate accurate modeling of the atmosphere, including solar radiative forcing. For the modern era this can be achieved by directly incorporating temporally extended space-borne spectral irradiance measurements, from the *Upper Atmosphere Research Satellite* (UARS) mission between 1991 and 2002 (Rottman *et al.*, 2001, Floyd *et al.*, 2002), by the *Variability of solar IRradiance and Gravity Oscillations* instrument (VIRGO) on the *SOlar and Heliospheric Observatory* (SOHO) since 1995 (Fröhlich *et al.*, 1997), by the *SOlar Radiation and Climate Experiment* (SORCE) experiment since 2004 (Harder *et al.*, 2010, Snow, McClintock, and Woods, 2012), and by the *PREcision MOnitor Sensor* (PREMOS) on PICARD since 2010 (Schmutz *et al.*, 2009), for example. However, when one wants to understand the processes involved during the Maunder Minimum, one must use reconstructed solar irradiance. Many approaches have been developed to generate such reconstructions; Thuillier *et al.* (2014) compared five of them on the basis of their absolute values, their relative variability for certain dates and their integrated flux in spectral bands relevant for climate modeling. These include the National Research Laboratory Solar Spectral Irradiance (NRLSSI) model (Lean, 2000a), which can produce reconstructions starting in 1610 between 120 nm and 100 µm, using solar images and the Ca II and Mg II indices. The Spectral And Total Irradiance REconstructions (SATIRE) model (Krivova, Vieira, and Solanki, 2010) allows reconstructions starting in 9500 BP between 120 nm and 160 µm with different proxies depending on the period and with full radiative transfer. The model described in Shapiro *et al.* (2011a; abbreviated SEA) also uses a radiative transfer code (COde for Solar Irradiance (COSI); Haberreiter, Schmutz, and Hubeny, 2008) for the reconstructions on the wavelength domain between 160 nm and 160 µm, starting in 7000 BP. Finally, the MaGnesium–Neutron Monitor (MGNM) model works in the UV only (120 – 400 nm), starting in 7000 BP, using the Mg II index and neutron monitor data. Good general agreement at the 5 to 10 % level is found between these various reconstructions as well as against observed spectra, for most of the wavelength range and dates examined. However, the associated differences in solar

heating rates predicted at a given date in the mesosphere turn out to be comparable with the heating rate differences between periods of low and high magnetic activities. This indicates that agreement at the 10 % level is not good enough for atmospheric/climate studies.

Thuillier's *et al.* (2014) study motivated the improvement of the original version of the Monte Carlo Spectral Solar Irradiance Model (MOCASSIM), as documented in Bolduc *et al.* (2012), which was included as one of the five reconstructions being tested. More specifically, studying them comparatively required extending MOCASSIM to shorter wavelengths, so as to be able to produce reconstructions in the spectral bands used for climate modeling, as well as to extend farther into the past, all the way to the 17th century Maunder Minimum. Both challenges were met successfully, and this paper documents these improvements, and presents in some detail solar UV spectral reconstructions for the Maunder Minimum epoch.

Section 2 presents a brief overview of the original MOCASSIM model for spectral irradiance between 200 and 400 nm for the period 1874 – 2010. The following sections describe the three primary improvements introduced into the model, namely the extension to shorter wavelengths (Section 3.1), the inclusion of a slowly-varying quiet-Sun component (Section 3.2), and the extension into the distant past using simulated sunspot emergences (Section 3.3). A reconstructed spectrum for 11 March 1992 is compared with the ATLAS-1 spectrum, observed on the same date, as a validation for our model (Section 4). Some representative spectral-flux times series and spectra are then presented in Section 5, focusing on a comparison of spectra representative of the Maunder Minimum epoch (averaged over the year 1680) and the Cycle 23 minimum (averaged over March 2009). We conclude in Section 6.

2. The Reconstruction Model

The MOCASSIM model (Bolduc *et al.*, 2012; hereafter Paper I) is an adaptation of the Crouch *et al.* (2008) model for total solar irradiance, which is a data-driven Monte Carlo simulation of solar active region emergence, fragmentation and erosion. Sunspots are "injected" into a synthetic solar surface on a one-day temporal cadence, with their observed heliographic location, area and time of emergence, in conjunction with a stochastic algorithm for introducing unobserved backside emergences. The decay of sunspots is modeled through a stochastic fragmentation cascade and boundary erosion, with fragments grouped into two size-based categories. Large-scale fragments are flagged as sunspots and/or pores, and continue to undergo fragmentation and erosion, while small-scale fragments are to become part of faculae and/or active network. See Section 2.2 of Crouch *et al.* (2008) for more details on this procedure and an extensive literature review justifying its assumptions. The contribution of the quiet-Sun network is modeled separately, as a stochastic emissivity component. The resulting time-evolving distribution of fragments is then used in a four-component model of the spectral solar irradiance:

$$S_\lambda(t) = S_{\lambda,Q}(t) + \sum_k \Delta S_{\lambda,S,k}(t) + \sum_j \Delta S_{\lambda,F,j}(t) + S_{\lambda,N}(t), \tag{1}$$

$$S_{\lambda,N}(t) = \alpha\big(1 - \beta A_{\mathrm{mag}}(t)\big) \cdot \big(S_\lambda(t) - \bar{S}_\lambda(t)\big) + \gamma |r_g|, \tag{2}$$

where $S_{\lambda,Q}$ is the quiet-Sun contribution, $\sum_k \Delta S_{\lambda,S,k}$ and $\sum_j \Delta S_{\lambda,F,j}$ are, respectively, the sum on each individual sunspot k and facula j contribution. The spots and facular contribution are calculated by multiplying their area, determined by the Monte Carlo simulation of

spot decay, with their contrasts, which are calculated with the procedures described below. The network contribution $S_{\lambda,N}$, as defined through Equation (2), includes an amplification of the rotational modulation represented by the α factor, weighted by the area occupied by the active region, $A_{\mathrm{mag}}(t)$. The β factor is an adjustable parameter scaling the amplitude of the weighting by the total active region areas. This term modulates an amplification of the deviation around the mean, represented by $S_\lambda(t) - \bar{S}_\lambda(t)$, where $\bar{S}_\lambda(t)$ is the smoothed irradiance time series, using an 81-day box-car average. It also includes a purely stochastic simulation of the network emissivity, where $|r_g|$ is a normally distributed random number of zero mean and unit variance, and γ is a wavelength-dependent parameter scaling the contribution. The optimization of the α, β and γ adjustable parameters is described in detail two paragraphs below.

The quiet-Sun emissivity is calculated by interpolating the monochromatic flux at the chosen wavelength on a reference spectrum representative of the Sun during low magnetic activity. A synthetic spectrum (Kurucz, 1993) was used in the original version of the model since it has the advantage of being completely free of magnetic structures, by design. Because the synthetic spectrum deviates significantly from observations below 200 nm, we chose to use an observed spectrum in this new version of the model.

The sunspot spectrum is approximated with a Kurucz's synthetic spectrum with $T_{\mathrm{e}} = 5250$ K, based on the effective average temperature of the umbrae and the penumbrae (respectively $T_{\mathrm{e}} \sim 4500$ K and $T_{\mathrm{e}} \sim 5400-5500$ K, Solanki and Unruh, 1998) and their area ratio of 1:3. This allows one to calculate the sunspot contrasts with the ratio of the monochromatic flux at $T_{\mathrm{e}} = 5250$ K and the flux of a quiet-Sun spectrum at $T_{\mathrm{e}} = 5750$ K. The facular and active network contribution is calculated by the method suggested in Solanki and Unruh (1998). First, the monochromatic flux is used to calculate an emission temperature *via* the black-body formula interpolated at the desired wavelength. This emission temperature is then used to calculate the photon formation height using the semi-empirical temperature profile "B" by Fontenla *et al.* (2009). Keeping the formation height fixed at that wavelength, interpolating their facular profile "P" yields a facular emission temperature, which is converted to spectral flux using the Planck formula. This emission temperature approach is implicitly based on the assumption of local thermodynamic equilibrium, which is known to break down for spectral domains formed high in the solar atmosphere. Solanki and Unruh (1998) could show that their procedure yields a satisfactory reproduction of ultraviolet radiative variability for wavelengths higher than 200 nm, provided that slight adjustments are made to the facular temperature profile (as discussed below). Moreover, the comparative exercise in spectrum reconstruction carried out by Thuillier *et al.* (2014) indicates that even in the 150 – 200 nm spectral range, the MOCASSIM spectral reconstructions compare as well to observations as other reconstructions taking into account non-local-thermodynamic-equilibrium (non-LTE) effects in their calculated spectra.

The free parameters of the model, such as α, β and γ, are adjusted simultaneously for 14 wavelengths (see Figure 1 for exact values) by minimizing the day-to-day squared difference between the model reconstructions and UARS data. After a few tests, it was determined that keeping the α and β parameters constant for every wavelength helped the convergence of the optimization runs, while maintaining accuracy. Simultaneously, we inverted an adjusted facular temperature profile using the optimal emission temperatures, namely the temperatures allowing the best reproduction of UARS variability for the 14 wavelengths. The simultaneous optimization of the free parameters and the adjusted facular temperature is necessary since the latter determines the variability amplitude over a cycle. This multi-objective fitting procedure involves minimizing the day-to-day squared difference between the model reconstructions and UARS data for the temperatures, whereas the α, β and γ parameters are

adjusted by minimizing the squared difference between the model and the observed residual distributions, which is a statistical representation of the deviations around the mean in the SSI time series (see Section 3 for more details). The optimization of the parameters and the facular temperature inversion are carried out by the genetic-algorithm (GA) based optimizer PIKAIA (Charbonneau and Knapp, 1995, Charbonneau, 2002). See Crouch *et al.* (2008) and Bolduc *et al.* (2012) for more details on the use of this procedure in this context, including explicit equations for the different χ^2 minimizations (see their Equations 10 – 12). The temperatures are then linearly interpolated between the optimal values to produce a newly derived temperature profile, which is used for the spectral reconstructions.

3. MOCASSIM 2.0

3.1. Extension to Shorter Wavelengths

The original MOCASSIM reconstructions are highly inaccurate at wavelengths below 200 nm, to a large extent because the baseline Kurucz (1993) synthetic spectrum differs greatly from observations below this limit (see Figure 2 in Bolduc *et al.*, 2012). We therefore opted to replace it by the ATLAS-3 spectrum, observed on 11 November 1994 near the activity minimum following Cycle 22. Even if it is not a truly non-magnetic spectrum, as the synthetic spectrum previously used, it is nevertheless a good representation of the Sun's emissivity for low magnetic activity. However, the calculation of photon formation heights with the black-body inversion procedure described previously yields different values from those calculated starting from the Kurucz spectrum, as expected from the different monochromatic fluxes at a given wavelength. Therefore, the facular temperatures obtained differ slightly but significantly from those optimized for the early version of the model, which leads to an erroneous reconstructed variability. We carried out a new inversion of an adjusted facular temperature profile using the same wavelengths, but starting with the ATLAS-3 spectrum. This new inversion now includes wavelengths below 200 nm to extend the model's spectral range. Figure 1a shows the different inverted temperature profiles in comparison with the original model for the faculae proposed by Fontenla *et al.* (2009). The very small error bars only reflect the intrinsic accuracy of the GA fitting procedure, and only demonstrate that the latter converges in a robust manner; no attempts were made to propagate measurement errors on the baseline spectrum through the reconstruction procedure.

The optimization was performed simultaneously for the optimal temperature and the amplitude of the network contribution, keeping the rotational modulation amplification factor and the active-region surface-coverage weighting factor constant. Figure 1b shows the optimal network factor (γ) as a function of wavelength, where it has been linearly interpolated between the wavelengths used for the optimization. Physical interpretation should not be ascribed to the non-monotonic variations with wavelength of our network emissivity parameter, as these simply reflect parameter values yielding the best fit for our specific choice for the stochastic model. We did verify that the peaks and troughs in the 220 – 280 nm wavelength range are not due to strong correlations with other fitted parameters, or with the facular temperature profile.

3.2. Quiet-Sun Variability

For the reconstructions spanning almost four centuries, it is necessary to take into account the contribution of a potential quiet-Sun variability. Other SSI reconstruction procedures

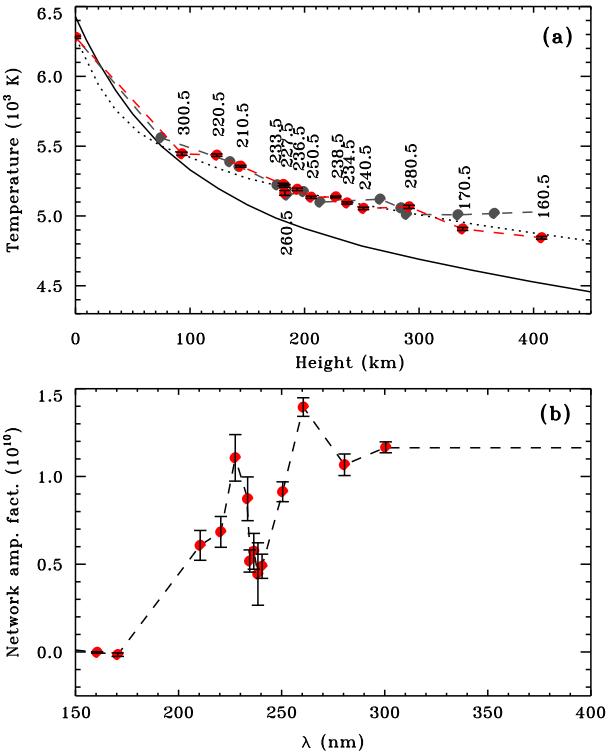

Figure 1 (a) Adjusted temperature profile, allowing the best fit to SOLSTICE/UARS data, for the updated version of MOCASSIM (red filled circles) with the error bars corresponding to the averaged revised temperature values plus or minus one standard deviation over the ten optimization runs. The red dashed line is the linearly interpolated temperature profile used for the reconstructions at other wavelengths. The black solid line is the Fontenla *et al.* (2009) profile for the quiet Sun, and the black dotted line is their profile for the faculae. The grey filled circles and dashed line is the Bolduc *et al.* (2012) temperature profile for the faculae. The wavelengths listed are 160.5, 170.5, 210.5, 220.5, 227.5, 233.5, 234.5, 236.5, 238.5, 240.5, 250.5, 260.5, 280.5, and 300.5. (b) The red filled circles represent the average optimal network amplification factor (γ) over ten optimization runs; their error bars are calculated in the same way as the facular temperatures. Once again, a linear interpolation between the optimal values is used for the reconstructions. This factor is kept constant between 300 and 400 nm because no optimization runs were performed in this interval due to the lack of precision of observed data.

include a long-term trend in solar variability. For example, Shapiro *et al.* (2011a) assumed that the minimum state of the quiet Sun in time corresponds to the quietest region on the present Sun. They used proxies such as ^{10}Be isotope concentration in ice cores and neutron-monitor data to interpolate between the current quiet-Sun level and the minimal quiet Sun. This long-term trend dominates the solar-cycle variability on secular time-scales and seems to be responsible for their very large historical variability in comparison with other models. The NRLSSI model uses a 15-year running mean of annual sunspot number coupled with a flux transport model to estimate the change in the quiet-Sun level. In a similar manner, a varying quiet-Sun component based on the radio flux at 10.7 cm ($F_{10.7}$) has been included in the MOCASSIM model.

Tapping *et al.* (2007) used the nonlinear relationship between $F_{10.7}$ and the sunspot number, calibrated between 1947 and now, to estimate the $F_{10.7}$ values since 1600. Since the

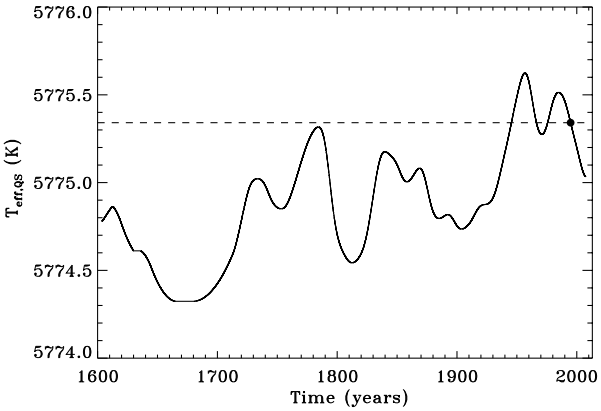

Figure 2 Quiet-Sun effective temperature inverted from the reconstructed TSI time series of Tapping *et al.* (2007). The dashed line shows the temperature corresponding to the date of observation of the ATLAS-3 spectrum.

$F_{10.7}$ is proportional the magnetic flux in active regions, it is used to estimate the total active region magnetic flux in the past. Then, the other magnetic flux components, such as faculae, are estimated with a simple cascade model. These are used to estimate the cyclic TSI variability. The secular irradiance component, which can be considered as a variation of the quiet-Sun level, is assumed to be due to a reservoir of subphotospheric magnetic flux modulating energy flow to the photosphere, causing small temperature variations and consequent small changes in irradiance. The subphotospheric magnetic flux is estimated with a smoothed total photospheric magnetic flux. Therefore, the low band-pass-filtered slowly varying component ($S_{10.7}$) of the $F_{10.7}$ radio flux allows a direct reconstruction of the quiet-Sun total irradiance, according to

$$I_{\odot}(t) = 0.017 S_{10.7}(t) + 1364.5, \tag{3}$$

where the constants 0.017 and 1364.5 are obtained using a regression analysis on the Physikalisch-Meteorologisches Observatorium Davos (PMOD) TSI composite (data set d41_61_0604).

An effective temperature is calculated for this irradiance assuming that it is emitted by a black body, as shown in Figure 2. Then, this temperature time series is compared with the effective temperature obtained for the value of $I_{\odot}$ for 11 November 1994, (corresponding to the observation of the ATLAS-3 spectrum) in the series. The result is a "correction" time series on the Sun's effective temperature, which we assumed to be caused by slow variations of the quiet-Sun emissivity. For the spectral irradiance reconstructions, we calculated an emission temperature for the monochromatic flux of the reference quiet-Sun spectrum (in this case, ATLAS-3) and we "corrected" it with the differences in effective temperatures calculated previously. It was then converted back to spectral flux with the Planck law.

3.3. Back to 1610

One of the most important motivations for the reconstruction of solar irradiance in the UV is for climate simulations during the Maunder Minimum. Other models based on sunspot number (SSN) successfully reconstructed total solar irradiance back to the Maunder Minimum, such as described in Krivova, Balmaceda, and Solanki (2007) and Lean *et al.* (2005). However, the MOCASSIM model necessitates data on sunspots emergences, area and position on the solar disk, which are not available for that period. We opted to develop a

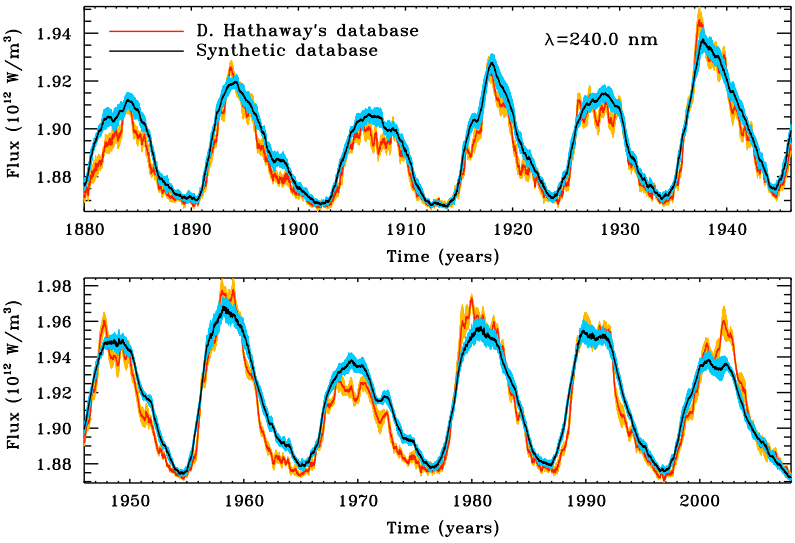

Figure 3 Comparison between reconstructed SSI at $\lambda = 240.0$ nm with the observed sunspot emergences extracted from the Greenwich database compiled by D. Hathaway (red solid line) and the synthetic emergences (black solid line). Both are over-plotted on the average of ten realizations plus or minus one standard deviation (in orange and light blue, respectively). The ten realizations are performed with different seeds for the random-number generator driving the backside emergences in the first case, and with ten distinct sunspot-emergence time series in the second. The results are smoothed with an 81-day box-car average before averaging over the ten realizations.

Monte Carlo model for synthetic emergences driven by the sunspot number time series (Lemerle *et al.*, 2014, private communication). Although developed independently, this procedure is conceptually quite similar to that described in Jiang *et al.* (2011). Calibration is carried out over the 1874 – 2011 interval using daily sunspot data compiled by D. Hathaway (http://solarscience.msfc.nasa.gov/greenwch.shtml), to establish the statistical properties of the spots' probability of emergence, area and location according to the phase of the cycle as determined from the SSN time series.

Figure 3 shows SSI reconstructions for the 1880 – 2008 interval using the real and synthetic emergences. The agreement is quite good for most of the time interval, with the amplitude, overall shape, and even substructure within individual cycles being well-reproduced. Significant deviations nonetheless exist, notably at the maximum of Cycles 14, 20, and 23 and during the descending phase of Cycles 19 and 20. These discrepancies are not due to the SSI reconstruction procedure itself, but can be traced directly to the simulated patterns of emergences used as its input data. Note also that the associated simulated SSN time series shows deviations with respect to the Zürich SSN time series at a level similar to that characterizing the Jiang *et al.* (2011) simulation protocol, about 1 % in the worst case, at the maximum of Cycle 23 (see Figure 3). These synthetic sunspot-emergence time series were used instead of the observed data to reconstruct SSI from 1610 to the present.

4. MOCASSIM 2.0: Validation

We first wish to validate our new inverted facular temperature profile for the whole wavelength range of interest by comparing our reconstructed time series with UARS/SOLSTICE

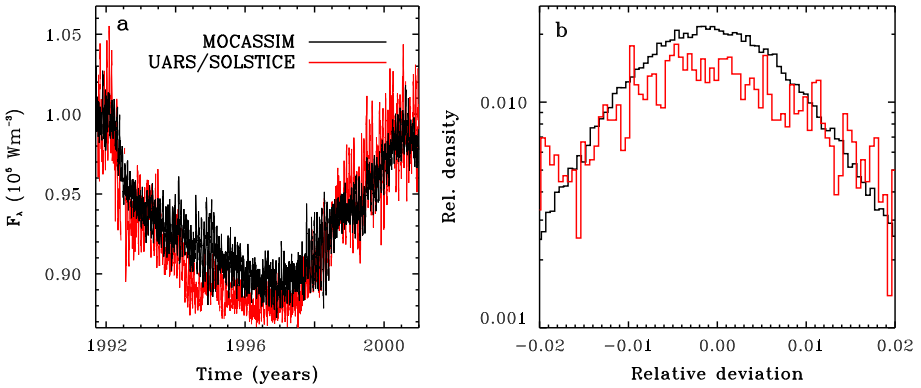

Figure 4 (a) Reconstruction of SSI at $\lambda = 150$ nm (in black) compared with UARS/SOLSTICE data (in red). (b) The distribution of the residuals for the model and the observations, being the difference between the original time series and the smoothed time series for every day, with the same color code. In panel (b), the x axis represents the relative deviation to the smoothed time series for a given day, and the y axis represents the fraction of days (over the whole time interval, roughly ten years) showing this specific deviation.

data between 1991 and 2002. In Figure 4, we show the reconstructed time series for $\lambda = 150$ nm, which is 10 nm below the smallest wavelength used for the temperature profile inversion. Considering this, the variability amplitude and the residual distribution are surprisingly well reproduced. The residual distribution is simply the distribution of the difference, for a given day, between the original SSI time series and its smoothed version, which is obtained with a 81-day box-car average. We used this distribution to optimize the parameters determining the amplification of the rotational modulation and the network weighting factor, by minimizing the square difference between the distribution of the observed residuals and the modeled residuals. The fit between the SSI time series and the residual distribution is very good for the wavelengths used for the optimization, as expected (this is not shown).

For further validation, we compared the reconstructed spectrum on a given day with available observations. Bolduc *et al.* (2012) compared a reconstructed spectrum with ATLAS-1, observed on 29 March 1992 (Thuillier *et al.*, 1998), between 200 and 400 nm. Figure 5 shows the ATLAS-1 spectrum (in red, $F_\lambda(\mathrm{AT1})$) and a reconstructed spectrum (in black, $F_\lambda(\mathrm{MOD})$) between 150 and 200 nm, including this time the quiet-Sun modulation, as described in Section 3.2. Because the two spectra are almost identical across the spectral range plotted, we also plot in blue their relative difference, defined here as

$$R(\mathrm{MOD{:}AT1}) = 2\frac{F_\lambda(\mathrm{MOD}) - F_\lambda(\mathrm{AT1})}{F_\lambda(\mathrm{MOD}) + F_\lambda(\mathrm{AT1})}. \tag{4}$$

This latter representation highlights differences hard to detect visually by direct comparison of the two spectra on the scale of Figure 5. In this wavelength range, our reconstructed spectrum generally overestimates the ATLAS-1 flux scale at the 3 to 5 % level. This systematic shift could be largely eliminated by lowering our quiet-Sun temperature by $\sim 6-8°$ K. This is much higher than the quiet-Sun temperature variability inferred from the Tapping *et al.* (2007) reconstruction, so the offset does not originate in our representation of the quiet-Sun secular variation. However, considering that the absolute uncertainty on the ATLAS-1 spectrum is about 3 % (Thuillier *et al.*, 2004), our reconstruction is still within the margin of error. Our reconstructed spectrum also underestimates the strength of many emission lines, notably at $\lambda \simeq 152.7$, 153.3, 154.8, 156.1, 164.0, 167.1, 180.8, and 181.7 nm, as indicated

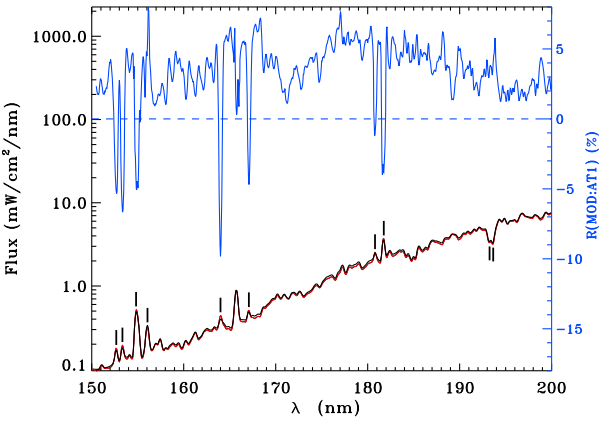

Figure 5 ATLAS-1 spectrum (in red) and reconstructed spectrum (in black) with the same resolution as ATLAS-1. The average plus or minus one standard deviation (calculated with the ten synthetic emergence realizations) is also plotted, but its width is smaller than the thickness of the black line. The relative percentage difference between the model and the observations is plotted in blue.

in Figure 5 by short vertical line segments. These are lines (or blends) of Si II, C IV, C I, Fe II, He II, and Al II, whose formation heights vary from the chromosphere, for Si II and Fe II (Doschek *et al.*, 1976), to the transition region, for C IV (Shine, Lites, and Chipman, 1978; Vernazza, Avrett, and Loeser, 1981; Fontenla *et al.*, 1999). Since our reconstruction scheme does not take into account non-LTE effects, which are essential for these lines, and our facular model only extends to the temperature minimum, these discrepancies are not surprising. That these lines appear in our spectrum is a direct consequence of our use of an observed spectrum as baseline. We also point out that the variability in absorption lines around 193.5 nm (a blend of Cr II, Fe II and Mn II around 193.25 nm and of Al I, Cr II and Co II around 193.65 nm),[1] forming lower down, is better reproduced.

At this juncture some technical issues are worth detailing. The reconstructed spectrum in Figure 5 was calculated (and plotted) using the same wavelength grid as ATLAS-1. Adopting a different wavelength scale would require, for comparison purposes, *e.g.*, evaluating Equation (4), an interpolation of one wavelength scale onto the other. In the early stages of the Thuillier *et al.* (2014) comparative exercise mentioned previously, it was quickly realized that the manner in which this interpolation is carried out can generate spurious oscillations in spectral ratio, of a magnitude similar to their true differences. The preferred strategy is obviously to use the same wavelength sampling as the observed spectrum, which is easy in the context of our reconstruction procedure. However, our baseline spectrum (here ATLAS-3) must then also be interpolated on the target wavelength grid. Various experiments revealed that a simple linear interpolation generally behaves best towards this end.

Finally, to validate our reconstructions starting in 1610, we followed Lean *et al.* (2005) and compared the flux variations integrated in spectral bands, between averages over the years 1713 and 1986. We reproduce in Table 1 their calculated values, obtained with two versions of their model, as described in Lean (2000a) and Wang, Lean, and Sheeley (2005). The former model infers the long-term trend in solar irradiance from brightness changes in Sun-like stars, and the latter by using a flux transport model to simulate the long-term evolution of the closed flux that generates faculae. For the 200 – 300 nm band, the variability obtained with MOCASSIM is slightly larger than the one obtained by Wang, Lean, and Sheeley (2005), which is itself larger than the earlier estimate of Lean (2000a). In the 315 – 400 nm band, MOCASSIM lies between the two. This comparison indicates that our reconstructions compare very well with other semi-empirical models.

[1] Atomic spectral line database, www.pmp.uni-hannover.de/cgi-bin/ssi/test/kurucz/sekur.html.

Table 1 Variations between the year 1713 and the year 1986 for two versions of the NRLSSI model and MOCASSIM. The MOCASSIM estimate is obtained with nine reconstructions using statistically different sunspot-emergence time series. The ratio has been calculated for these nine reconstructions, then averaged. The standard deviation in the ratio is used as an error estimate in the reconstruction procedure, which is dominated by the variation in backside sunspot emergence.

Spectral band (nm)	Lean (2000a)	Wang, Lean, and Sheeley (2000a)	MOCASSIM
200 – 300	0.9864	0.9957	0.9961 ± 0.0003
315 – 400	0.9968	0.9990	0.9980 ± 0.0001

5. MOCASSIM 2.0: Results

Figure 6 shows the average of ten reconstructions at $\lambda = 240.5$ nm and $\lambda = 370.5$ nm produced with ten statistically independent realizations of the sunspot synthetic emergence simulation (using different seeds for the random number generator). The average of the ten reconstructions is illustrated along with its value plus or minus one standard deviation, smoothed with an 81-day boxcar average, plotted in black in the top panels. In most cases, these "error bars" are smaller than the thickness of the line. The quiet-Sun contribution is also plotted in green. The lower panels show the facular brightening (in red), the spot darkening (in dark blue) and the daily, random network contribution in light blue.

Several features in Figure 6 deserve explicit mention. First, the relative contribution of quiet-Sun variations to the overall cycle-to-cycle variability is more pronounced at long wavelengths, even though the absolute flux variations are proportionally larger at shorter wavelengths. Second, during the Maunder Minimum but also in the minima following low-amplitude cycles, such as during the 1800 – 1825 Dalton Minimum, as well as in the recent extended minimum preceding Cycle 24, the network contribution is seen to dominate the emissivity at all wavelengths. Because the facular elements in our surface magnetic-flux evolution model decay on a relatively long timescale ($\sim$ 92 days, Crouch *et al.*, 2008), their emissivity contribution still dominates in the minimum phases following high-amplitude cycles. This is shown more explicitly in Figure 7 for the same wavelengths, for four periods of low activity, including the complete year 1680 representing the Maunder Minimum, May 1996 for the Cycle 22 minimum, May 2008 and March 2009 for the descending phase and minimum of Cycle 23. The contributions from the network, the faculae and the spots are illustrated in light blue, red, and dark blue, respectively. This clearly shows that the dominant contribution during the Maunder Minimum was coming from the network, whereas the faculae and spots still contributed during the recent minima. We can see the decreasing amplitude of facular and spot contributions between May 2008 and March 2009, as could be expected if we consider the latest period to be corresponding to the minimum of Cycle 23. In summary, according to our model, during the last minimum the Sun did not reach as quiescent a state as it did during the Maunder Minimum. A similar conclusion was reached by Thuillier *et al.* (2012) with their reconstruction based on the Mg II index.

The reconstruction of two spectra representative of the Maunder Minimum and of the Cycle 23 minimum allows a more detailed comparison between these two periods. In the first case, we used a spectrum averaged over March 2009 and in the second case, we averaged over the whole year 1680. Both spectra were calculated with the variable quiet-Sun as described in Section 3.2, and with the constant quiet-Sun from the ATLAS-3 spectrum. Figure 8 shows the reconstructed spectra for both periods, now over the full reconstructed wavelength interval 150 – 400 nm, and using the variable quiet-Sun. The difference between the two spectra varies from about 0.7 % at the short-wavelength end of the range, down to

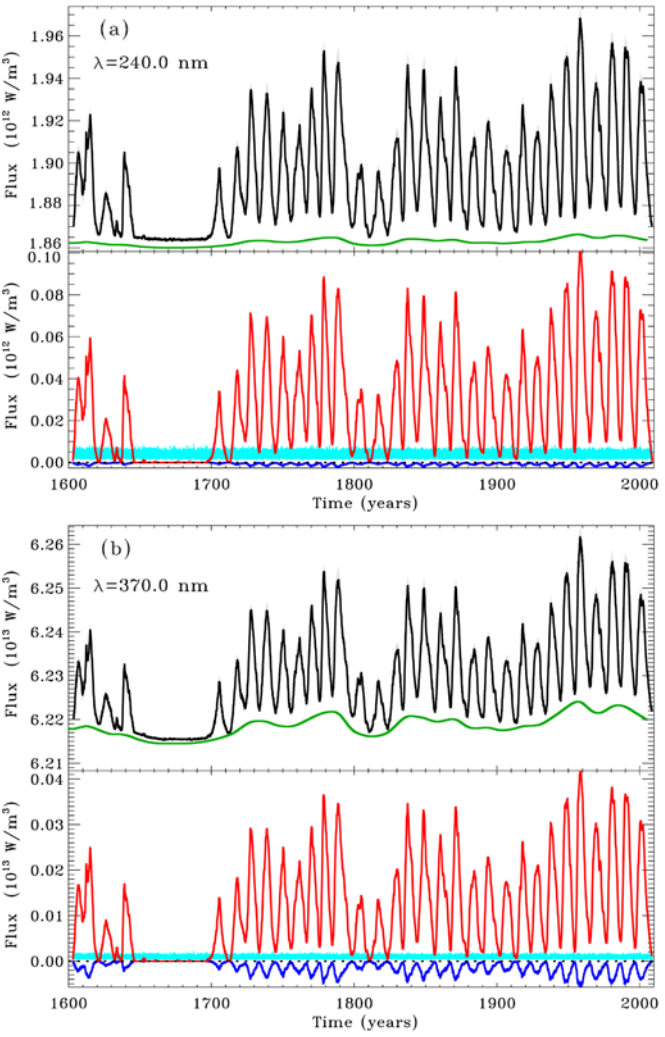

Figure 6 The average of ten reconstructions using ten different synthetic sunspot-emergence time series, for $\lambda = 240.5$ nm (a) and $\lambda = 370.5$ nm (b), is illustrated by the solid black curves. The grey area, which is similar to the thickness of the curve itself and thus hardly visible, represents the average plus or minus one standard deviation. The color curves separate the various contributions to the SSI: the quiet-Sun contribution is plotted in green (upper panels), while in the lower panels the random contribution from the network, weighted by the wavelength dependent factor showed in Figure 1, is plotted in light blue. The red and deep blue curves are the facular and spot contributions to the SSI, respectively.

0.1 % at longer wavelengths, and so is too small to be apparent in the logarithmic scale of this plot. We opted again to over-plot their relative difference, as defined by Equation (4) (right vertical axis and blue line). We also calculated the same relative difference between the two spectra, but now in a reconstruction using a temporally constant quiet-Sun (green curve). Comparing the blue and green curves thus indicates that the differences between the 2009 and the 1680 spectra are primarily due to our quiet-Sun variability for wavelengths longer than 300 nm, but not at shorter wavelengths. Evidently, in 2009 there remained suffi-

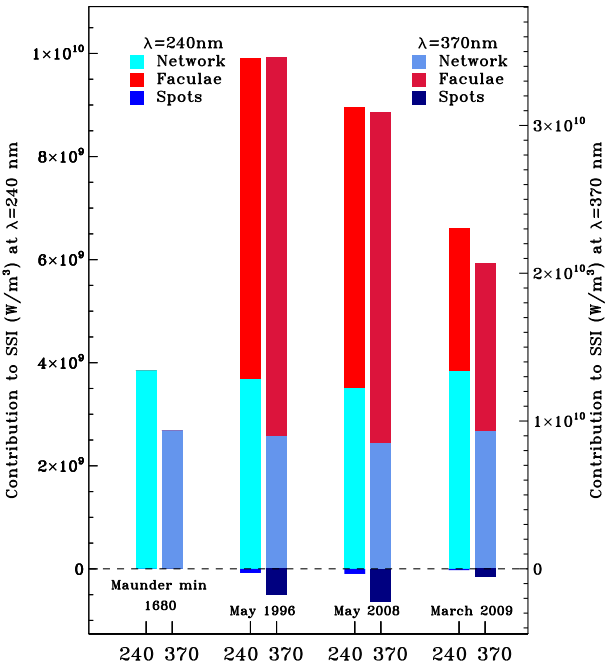

Figure 7 Contributions from the network, the faculae, and the spots for four periods of low activity for the year 1680 (Maunder Minimum), May 1996 (minimum of Cycle 22), May 2008 (descending phase of Cycle 23), and March 2009 (minimum of Cycle 23). The wavelengths 240 and 370 nm are considered. The left-hand side axis and bars correspond to $\lambda = 240$ nm, and the right-hand side axis and bars to $\lambda = 370$ nm. This clearly shows that the network was the only component contributing to the irradiance (along with the quiet Sun, of course) during the Maunder Minimum, whereas the faculae and spots played a more important role during the modern minima. Their contribution decreased between 2008 and 2009, but some faculae and spots remained nonetheless during this especially long minimum.

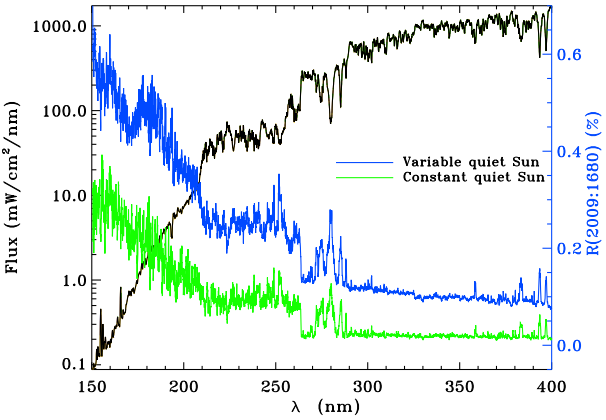

Figure 8 Reconstructed solar spectra, with varying quiet Sun, averaged over March 2009 and over the whole year 1680 (they are indistinguishable in the logarithmic scale). Their percentage relative difference is plotted in blue. For comparison, the relative difference of the same spectra calculated with a constant quiet-Sun is plotted in green. This clearly shows that the difference between the emissivity during the Maunder Minimum and the 2009 minimum is not only caused by a variation of the quiet Sun, but seems to depend also on remnant magnetic structures such as faculae and the quiet network, which were still present in 2009.

cient decay elements from active regions to produce significant emissivity above quiet-Sun levels, this being most prominent at short wavelengths due to the spectral dependency of the facular and network contribution.

6. Discussion and Conclusions

We described and documented the latest series of improvements made in the MOCASSIM model (Bolduc *et al.*, 2012), a fast model for reconstructing spectral irradiance in the near- and mid-ultraviolet. The primary improvements are i) the extension to shorter wavelengths, ii) the addition of a secular modulation of the quiet-Sun emissivity, and iii) the extension of the reconstructed time interval back to the beginning of the 17th century. The model can now be used for spectral reconstructions between 150 and 400 nm using a new inverted temperature profile for the faculae, optimized using the ATLAS-3 spectrum as a baseline for the quiet-Sun emissivity. The quiet-Sun long-term modulation was calculated with an effective temperature correction on the quiet-Sun emissivity estimated from a TSI reconstruction based on $S_{10.7}$ according to Tapping *et al.* (2007). In the time period before 1874, *i.e.*, prior to the beginning of the Greenwich photographic sunspot database, a Monte Carlo model driven by the SSN time series was used (Lemerle *et al.*, 2014, private communication, and also Jiang *et al.*, 2011). This improved version of the MOCASSIM model can reproduce UARS/SOLSTICE irradiance time series and the residual distribution for wavelengths as low as 150 nm. It can reproduce the ATLAS-1 spectrum observed on 29 March 1992, to an accuracy of 5 % or better between 150 and 400 nm, the largest deviation occurring in emission lines formed in the chromosphere or transition region, which is expected given the design of the model, which lacks a chromosphere.

These improvements were motivated in part by the comparative study of Thuillier *et al.* (2014), who could show that the MOCASSIM 2.0 reconstructions described in this article have an accuracy similar to other existing protocols, namely SATIRE (Krivova, Vieira, and Solanki, 2010), SEA (Shapiro *et al.*, 2011b), NRLSSI (Lean, 2000a), and MGNM (Thuillier *et al.*, 2012). This study showed that the fluxes calculated with the MOCASSIM model agree within 5 % with the values calculated with the NRLSSI (Lean, 2000b) and the MGNM (Thuillier *et al.*, 2012) models after 1874.

We have produced reconstructed SSI UV time series extending back to 1610, as well as a mean spectrum for the year 1680, in the middle of the Maunder Minimum. During that time period, our reconstructions suggest that the network is the primary contributor to the UV emissivity in the mid-UV (150 – 300 nm), while the variation of the quiet-Sun emissivity dominates in the near-UV (300 – 400 nm). We also compared this spectrum with a mean spectrum for March 2009, during the extended activity minimum between Cycles 23 and 24. Taken at face value, this comparative exercise suggests that in the mid-UV the emissivity was still higher in 2009 than in the Maunder Minimum, but only at the 1 % level. Roughly two thirds of that excess can be traced to our quiet-Sun emissivity variation, while in the near-UV the latter is responsible for the whole excess emissivity above Maunder Minimum emissivity.

Acknowledgements We thank Gerard Thuillier for kindly making available his full solar spectra from ATLAS-1 and ATLAS-3, as well as for numerous useful discussions. We also thank Ken Tapping for providing his updated sequence of $S_{10.7}$. This work was supported by Canada's Natural Sciences and Engineering Research Council, Research Chair Program, the Programme de Recherche en Équipe of the Fonds de Recherche sur la Nature et Technologie (Québec, Grant 119078), as well as by the Space Science Enhancement Program of the Canadian Space Agency (Grant 9SCIGRA-21).

References

Bolduc, C., Charbonneau, P., Dumoulin, V., Bourqui, M.S., Crouch, A.D.: 2012, A fast model for the reconstruction of spectral solar irradiance in the near- and mid-ultraviolet. *Solar Phys.* **279**, 383.

Charbonneau, P.: 2002, An introduction to genetic algorithms for numerical optimization. *NCAR Technical Note 450+IA*, 311.

Charbonneau, P., Knapp, B.: 1995, A user's guide to PIKAIA 1.0. *NCAR Technical Note 418+IA*, 311.

Crouch, A.D., Charbonneau, P., Beaubien, G., Paquin-Ricard, D.: 2008, A model for the total solar irradiance based on active region decay. *Astrophys. J.* **677**, 723.

Doschek, G.A., Feldman, U., VanHoosier, M.E., Bartoe, J.-D.F.: 1976, The emission-line spectrum above the limb of the quiet Sun: 1175 – 1940 Å. *Astrophys. J. Suppl. Ser.* **31**, 417.

Floyd, L.E., Prinz, D.K., Crane, P.C., Herring, L.C.: 2002, Solar UV irradiance variation during cycle 22 and 23. *Adv. Space Res.* **29**, 1957.

Fontenla, J.M., White, O.R., Fox, P.A., Avrett, E.H., Kurucz, R.L.: 1999, Calculation of solar irradiances. I. Synthesis of the solar spectrum. *Astrophys. J.* **518**, 480.

Fontenla, J.M., Curdt, W., Haberreiter, M., Harder, J., Tian, H.: 2009, Semiempirical models of the solar atmosphere. III. Set of non-LTE models for far-ultraviolet/extreme-ultraviolet irradiance computation. *Astrophys. J.* **707**, 482.

Forster, P., Ramaswamy, V., Artaxo, P., Bernsten, T., Betts, R., Fahey, D.W., Haywood, J., Lean, J., Lowe, D.C., Myhre, G., Nganga, J., Prinn, R., Raga, G., Schulz, M., Dorland, R.V.: 2007, Changes in atmospheric constituents and in radiative forcing. In: Solomon, S., Qin, D., Manning, M., Chen, Z., Marquis, M., Averyt, K.B., Tignor, M., Miller, H.I. (eds.) *Climate Change 2007: The Physical Science Basis. Contribution of Working Group I to the Fourth Assessment Report of the Intergovernmental Panel on Climate Change*, Cambridge University Press, Cambridge, 188.

Fröhlich, C., Crommelynk, D.A., Wehrli, C., Anklin, M., Dewitte, S., Fichot, A., Finsterle, W., Jiménez, A., Chevalier, A., Roth, H.: 1997, In flight performance of the VIRGO solar irradiance instruments on SOHO. *Solar Phys.* **175**, 267.

Gray, L.J., Beer, J., Geller, M., Haigh, J.D., Lockwood, M., Matthes, K., Cubasch, U., Fleitmann, D., Harrison, G., Hood, L., Luterbacher, J., Meehl, G.A., Shindell, D., van Geel, B., White, W.: 2010, Solar influence on climate. *Rev. Geophys.* **48**, RG4001.

Haberreiter, M., Schmutz, W., Hubeny, I.: 2008, NLTE model calculations of the solar atmosphere with an iterative treatment of opacity distribution functions. *Astron. Astrophys.* **492**, 833.

Haigh, J.D., Winning, A.R., Toumi, R., Harder, J.W.: 2010, An influence of solar spectral variations on radiative forcing of climate. *Nature* **467**, 696.

Harder, J.W., Thuillier, G., Richard, E.C., Brown, S.W., Lykke, K.R., Snow, M., McClintock, W.E., Fontenla, J.M., Woods, T.N., Pilewski, P.: 2010, The SORCE SIM solar spectrum: comparison with recent observations. *Solar Phys.* **263**, 3.

Jiang, J., Cameron, R.H., Schmitt, D., Schüssler, M.: 2011, The solar magnetic field since 1700. I. Characteristics of sunspot group emergence and reconstruction of the butterfly diagram. *Astron. Astrophys.* **528**, A82.

Krivova, N.A., Balmaceda, L., Solanki, S.K.: 2007, Reconstruction of solar total irradiance since 1700 from the surface magnetic flux. *Astron. Astrophys.* **467**, 335.

Krivova, N.A., Vieira, L.E.A., Solanki, S.K.: 2010, Reconstruction of solar spectral irradiance since the Maunder minimum. *J. Geophys. Res.* **115**, A12112.

Kurucz, R.L.: 1993, Models. ftp.stsci.edu/cdbs/grid/k93models/kp00/.

Lean, J.: 2000a, Evolution of the Sun's spectral irradiance since the Maunder Minimum. *Geophys. Res. Lett.* **27**, 2425.

Lean, J.: 2000b, Short-term, direct indices of solar variability. *Space Sci. Rev.* **94**, 39.

Lean, J., Rottman, G., Harder, J.W., Kopp, G.: 2005, SORCE contribution to new understanding of global change and solar variability. *Solar Phys.* **230**, 27.

Rottman, G.J., Woods, T.N., Snow, M., de Toma, G.: 2001, The solar cycle variation in ultraviolet irradiance. *Adv. Space Res.* **27**, 1927.

Schmutz, W., Fehlmann, A., Hülsen, G., Meindl, P., Winkler, R., Thuillier, G., Blattner, P., Buisson, F., Egorova, T., Finsterle, W., Fox, N., Gröbner, J., Hochedez, J.-F., Koller, S., Meftah, M., Meisonnier, M., Nyeki, S., Pfiffner, D., Roth, H., Rozanov, E., Wehrli, C., Werner, L., Wyss, J.U.: 2009, The PREMOS/PICARD instrument calibration. *Metrologia* **46**, 202.

Shapiro, A.I., Schmutz, W., Rozanov, E.V., Schoell, M., Haberreiter, M., Shapiro, A.V., Nyeki, S.: 2011a, A new approach to long-term reconstruction of the solar irradiance leads to large historical solar forcing. *Astron. Astrophys.* **529**, 67.

Shapiro, A.V., Rozanov, E.V., Egorova, T.A., Shapiro, A.I., Peter, T., Schmutz, W.: 2011b, Sensitivity of the Earth's middle atmosphere to short-term solar variability and its dependance on the choice of solar irradiance data set. *J. Atmos. Solar-Terr. Phys.* **73**, 348.

Shine, R.A., Lites, B.W., Chipman, E.G.: 1978, Overlapping emission peaks in the solar C I multiplets at λ1560 and λ1657. *Astrophys. J.* **224**, 247.

Snow, M., McClintock, W.E., Woods, T.N.: 2012, Solar spectral irradiance variability in the ultraviolet from SORCE and UARS SOLSTICE. *Adv. Space Res.* **46**, 296.

Solanki, S.K., Unruh, Y.C.: 1998, A model of the wavelength dependence of solar irradiance variations. *Astron. Astrophys.* **329**, 747.

Tapping, K., Boteler, D., Charbonneau, P., Crouch, A., Manson, A., Paquette, H.: 2007, Solar magnetic activity and total solar irradiance since the Maunder Minimum. *Solar Phys.* **246**, 309.

Thuillier, G., Hersé, M., Simon, P.C., Labs, D., Mandel, H., Gillotay, D.: 1998, Observation of the solar spectral irradiance from 200 nm to 870 nm during the ATLAS 1 and ATLAS 2 missions by the SOLSPEC spectrometer. *Metrologia* **35**, 689.

Thuillier, G., Hersé, M., Labs, D., Foujols, T., Peetermans, W., Gillotay, D., Simon, P.C., Mandel, H.: 2003, The solar spectral irradiance from 200 to 2400 nm as measured by the SOLSPEC spectrometer from the ATLAS and EURECA missions. *Solar Phys.* **214**, 1.

Thuillier, G., Floyd, L., Woods, T.N., Cebula, R.P., Hilsenrath, E., Hersé, M., Labs, D.: 2004, Solar irradiance reference spectra for two solar active levels. *Adv. Space Res.* **34**, 256.

Thuillier, G., DeLand, M., Shapiro, A., Schmutz, W., Bolsée, D., Melo, S.: 2012, The solar spectral irradiance as a function of the Mg II index for atmosphere and climate modeling. *Solar Phys.* **277**, 245.

Thuillier, G., Melo, S.M.L., Lean, J., Krivova, N.A., Bolduc, C., Fomichev, V.I., Charbonneau, P., Shapiro, A.I., Schmutz, W., Bolsée, D.: 2014, Analysis of different spectral irradiance reconstructions and their impact on solar heating rates calculations. *Solar Phys.* **289**, 1115.

Vernazza, J.E., Avrett, E.H., Loeser, R.: 1981, Structure of the solar chromosphere. III. Models of the EUV brightness components of the quiet Sun. *Astrophys. J. Suppl. Ser.* **45**, 635.

Wang, Y.-M., Lean, J.L., Sheeley, N.R.: 2005, Modeling the Sun's magnetic field and irradiance since 1713. *Astrophys. J.* **625**, 522.